

Application of a Semi-Empirical Method to Model Subsonic Vortex Lift over Sharp Leading-Edge Delta Wings

Daniel Huynh, Davide Di Pasquale and Simon A. Prince
*School of Aerospace, Transport & Manufacturing, Cranfield University, Cranfield,
Bedfordshire, UK*

Vivek Ahuja
Research in Flight, Austin, Texas, USA

A semi-empirical method is applied as a complement to the FlightStream solver, to more accurately model subsonic vortex lift over a sharp leading-edge delta wing. The method, based on the prediction of flow patterns and the application of the Polhamus method, is particularly well-adapted to a preliminary aerodynamic design phase. Within a few minutes, it can accurately predict the aerodynamic forces generated by the flow over a delta wing, which are strongly affected by the presence of a leading-edge vortex. This study presents a detailed analysis where computed results are compared against experimental data. Those were obtained from a test case of a 65° subsonic delta wing experiment (case 1), along with a sensitivity analysis against sweep angle and aspect ratio where multiple subsonic delta wings were tested (case 2). A good agreement is observed between computed data and experimental results, within pre-stall, before the vortex bursts. Analysed results demonstrate the validity of the method, for multiple wing configurations associated with different flow conditions.

I. Nomenclature

$AoA-\alpha$	= Angle of Attack (degrees)	M	= Mach Number
AR	= Aspect Ratio	mac	= Mean Aerodynamic chord (m)
b	= wingspan (m)	Re	= Reynolds Number
CAD	= Computer-Aided Design	s	= direction along the local surface
C_A	= axial force coefficient	S_{ref}	= Wing reference area (m ²)
C_D	= drag force coefficient	t	= maximum wing thickness (m)
C_{D0}	= boundary-layer drag force coefficient	t/c	= thickness to chord ratio
C_{Di}	= lift-induced drag force coefficient	U_e	= local streamline velocity (m/s)
C_{F_x}	= local skin friction drag force coefficient	V	= freestream velocity (m/s)
C_L	= lift force coefficient	V_N	= blowing velocity (m/s)
C_{Lv}	= vortex lift force coefficient	δ^*	= displacement thickness (m)
C_N	= normal force coefficient	μ	= dynamic viscosity (N.s/m ²)
C_p	= pressure coefficient	ρ	= flow density (kg/m ³)
c_r	= root chord (m)	ω	= downwash velocity (m/s)
D	= induced drag (N)	Γ	= Aerodynamic circulation
d	= sting diameter (m)	Λ_{LE}	= leading-edge sweep angle
K_v	= constant of proportionality in the vortex lift equation		

II. Introduction

To achieve a good balance between supersonic cruise performance and manoeuvrability at supersonic speeds, highly swept delta wings are often the chosen planform. The flow around a delta wing is characterised by strong vortices produced by the body flying at a low to medium angle of attack. This vortex suction generates a considerable part of the overall lift of the wing. The studies of the flow's behaviour over delta wings have been conducted with

deep interest as aerodynamicists are looking to generate large amounts of lift force at high angles of attack. Considering a conventional wing, the maximum lift is reached at a moderate angle of attack limited by the phenomenon of stall. From this angle of attack, the flow on the suction side cannot stay attached to the surface, resulting in a loss of suction and a severe drop in lift force.

Because of its specific geometry, a delta wing can reach a much higher angle of attack before stalling, generating a larger amount of lift force. Once the flow reaches the sharp leading-edge of the wing and separates, the separated flow rolls up inboard to form a primary vortex above the wing. Once fully formed, the primary vortex interacts with the boundary layer, promoting secondary crossflow separation. This results in the appearance of a minor co-rotating vortex, called the secondary vortex [1]. The swirling motion of the vortex core generates an additional suction force on the upper surface near the leading-edge, causing an increase in lift generation [2]. The vortices keep increasing in both strength and size, until a sudden change in the vortex structure, leading to a sudden dissipation of the vortex energy, defined as a vortex burst. The suction generated over the surface then drops causing the stall of the delta wing [3].

During conceptual and preliminary aerodynamic design phases, low-order methods are usually used to compute multiple flow solutions without requiring high computational resources and time, due to the large number of iterations required. But it can be difficult for such methods to model the phenomenon of vortex interaction with the flow over a delta wing, due to its complexity [4]. Therefore, this study aims to assess the accuracy of a semi-empirical method, applied to model the additional lift, and drag components due to the presence of vortices over a sharp leading-edge delta wing at subsonic speed. Coupled with FlightStream, a solver capable of computing accurately the aerodynamic forces, generated under inviscid flow assumptions, the overall method predicts the lift and drag forces generated by a delta wing, for a large range of flow conditions, including the effects of vortex suction.

The results obtained from the semi-empirical method were compared to subsonic experimental data collected for a 65° sweep symmetrical delta wing (case 1) [5]. The experiments were performed in a low subsonic wind tunnel, at a Mach Number of $M = 0.133$ and a Reynolds Number of $Re_{mac} = 10^6$ [6].

Furthermore, to test the sensitivity of such method against aspect ratio and sweep angle, multiple analyses were performed using a family of six other delta wings with available experimental data. Those wings were tested in a low turbulence wind tunnel, at a fixed velocity of $V = 30.5 \text{ m/s}$ for a range of different Reynolds numbers, based on the aerodynamic mean chord, from $Re_{mac} = 0.25 \times 10^6$ to $Re_{mac} = 0.5 \times 10^6$ (case 2) [7].

III. Geometry

The first case focuses on the analysis of a model composed of a 65° sweep angle delta wing, with a sharp leading-edge [6]. The wing was linked to a mechanical arm by a sting, connected along the symmetrical axis of the wing. The model schematics are illustrated in Fig.1 while Fig.2 shows the test configuration in a wind tunnel. Table 1 summarizes the model reference values. For the second case, six cambered delta wings were investigated, having sharp leading edges with sweep angles ranging from 45° to 76° . The wings have the same planform area of $S_{ref} = 0.032 \text{ m}^2$, with centre-line chords varying from 0.179m to 0.359m [7]. Figure 3 shows the different model schematics and Table 2 provides the reference values.

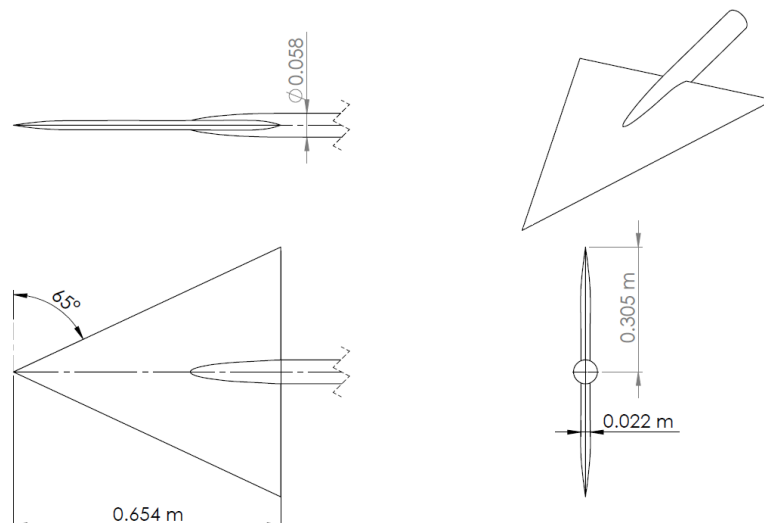


Fig. 1 Case 1: Schematics of the 65° sharp leading-edge delta wing.

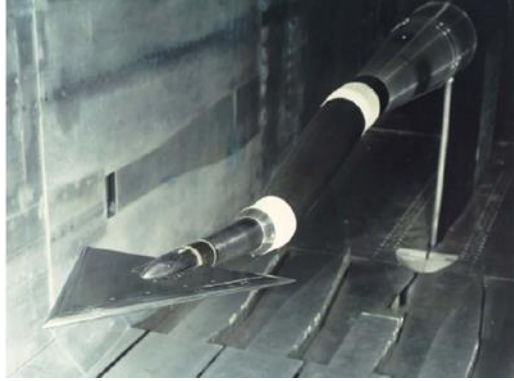


Fig. 2 Case 1: a 65° delta wing in its test configuration and the support system [6].

Table. 1 Case 1: 65° delta wing reference dimensions [6].

Dimension	Acronym	Value
root chord	c_r	0.654 m
wingspan	b	0.610 m
maximum wing thickness	t	0.022 m
sting diameter	d	0.058 m
reference area	S_{ref}	0.1993 m ²
mean aerodynamic chord	mac	0.4358 m

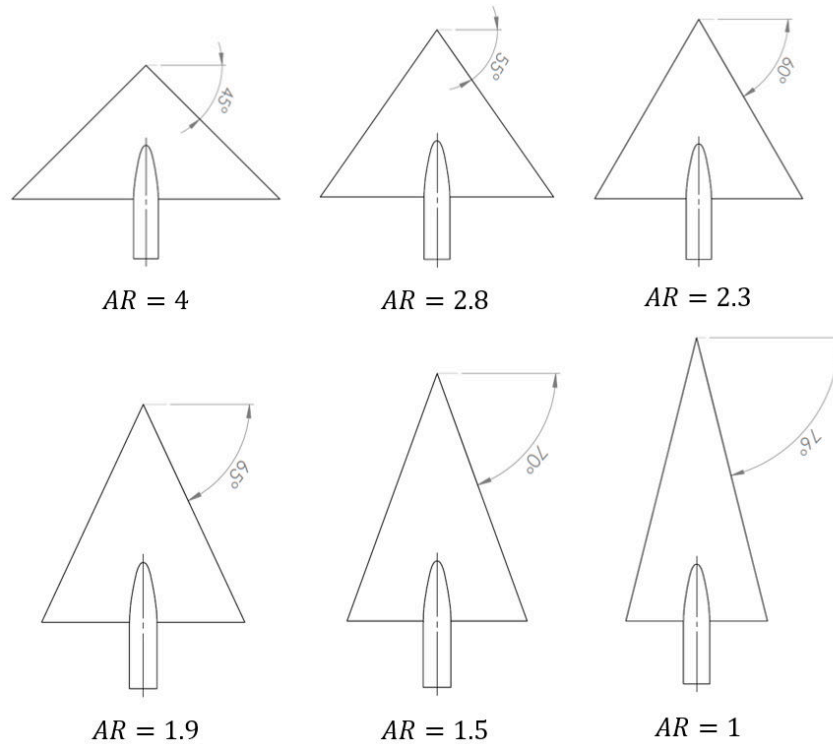


Fig. 3 Case 2: Schematics of the different sharp leading-edge delta wings for further analysis.

Table. 2 Case 2: Reference dimensions for different delta wings.

LE sweep angle Λ_{LE}	45°	55°	60°	65°	70°	76°
root chord c	0.179 m	0.215 m	0.236 m	0.263 m	0.298 m	0.359 m
wingspan b	0.359 m	0.300 m	0.273 m	0.245 m	0.217 m	0.179 m
Aspect Ratio AR	4	2.8	2.3	1.9	1.5	1
thickness to chord ratio t/c	6%					
reference area S_{ref}	0.032 m ²					

IV. Digital Model

The two distinctive elements that formed the original geometry have been generated using SolidWorks, from the initial dimensional specifications. Only half of the model was created since a symmetry boundary condition can be applied to the geometry. The CAD files were then exported to FlightStream to process the meshing. Different meshing strategies were adopted according to the nature of the body.

For a bluff body, such as the sting, the *Wrapper* operation was used to mesh the component. This tool “shrink-wrapped” a water-tight surface mesh around the geometry component, cleaning potentially poor topology CAD model and detailing features for fluid flow analysis. This enabled the orientation of the mesh along the flow direction, improving the mesh's capability to capture the flow features over the body. The sting's mesh was locally refined at the nose, to improve the mesh in a region of high curvature and flow gradients, as shown in Fig. 4a.

For the wing, which can be considered as a complex swept body, the *Aligned Mesher* was used to generate the meshing. This created an anisotropic mesh that can be controlled in chordwise and spanwise directions. The parameters of the mesh, such as the number of subdivisions both chordwise and spanwise or the growth pattern, were chosen to enable a mesh refinement near the leading-edge and the trailing-edge. This enabled a proper capture of the curvature and any corresponding phenomenon while preserving a good mesh quality regarding its aspect ratio and its skewness, as shown in Fig. 4b.

A *Boolean Unite* operation was then performed to merge the two components into a single body. Figure 4c illustrates the unite operation and Fig. 4d shows the model with a symmetrical condition applied.

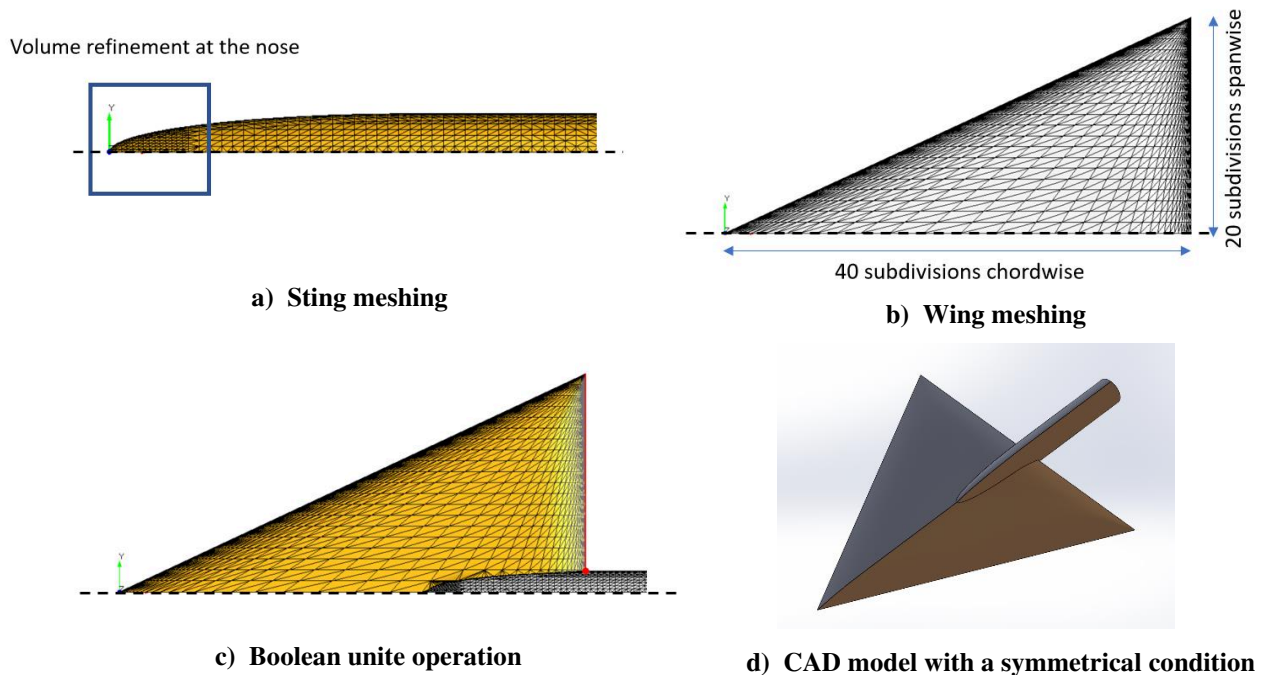


Fig. 4 Mesh visualization of the model sting + delta wing.

V. FlightStream Surface Vorticity Solver

FlightStream, developed by Dr Vivek Ahuja since 2013, is a robust and efficient vorticity-based flow solver, capable of modelling compressible and incompressible flow solutions at a speed up to the critical Mach Number. The solver is particularly efficient for conceptual and preliminary aerodynamic design studies, due to its rapidness and accuracy in computing inviscid flows.

FlightStream solver depends on the estimation of the circulation around a specific geometry. Therefore, it is based on the Kutta-Joukowski equation, applied to each panel, to evaluate the induced aerodynamic loads [8]. As such, it used the principle of vortex rings over the surface cells to evaluate the velocity induced by such vortex rings at any point around the body [9]. Once the distribution of velocity along vertices is known for a given section, the corresponding integrated circulation can be calculated using the Stokes theorem:

$$\Gamma_k = \int_0^L V_{induced,l} \cdot dl \quad (1)$$

Since the body is three-dimensional, the Kutta-Joukowski theorem cannot be directly applied. Therefore, different sections needed to be created, normal to the direction of the flow, to enclose the body into an effective box of sectional planes [10].

The induced lift can therefore be evaluated for each plane, in the span-wise direction, using the Kutta-Joukowski equation, defining it as:

$$L_i = \int_{-\frac{b}{2}}^{\frac{b}{2}} \rho_{\infty} V_{\infty} \Gamma_y dy \quad (2)$$

Furthermore, the alignment of the planes is similar to a lifting-line distribution of integrated vorticity along a rectangular wing. Therefore, using the Prandtl lifting line theory which assimilates each cross-section vorticity to a horseshoe-shaped vortex, the downwash velocity and the induced drag can be evaluated as:

$$\omega_y = \frac{1}{4\pi} \int_{-\frac{b}{2}}^{\frac{b}{2}} \left(\frac{1}{y - y_0} \right) \frac{-d\Gamma_{y_0}}{dy} dy_0 \quad (3)$$

$$D_i = \int_{-\frac{b}{2}}^{\frac{b}{2}} \rho_{\infty} \omega_{\infty} \Gamma_y dy \quad (4)$$

The evaluation of skin-friction drag is based on the estimation of the local Reynolds Number for each cell. Since FlightStream does not compute velocity at each cell, the local Reynolds Number needs to be estimated using the local vorticity as:

$$Re = \frac{\rho_{\infty} V_{\infty} \left(x + \frac{y}{V_{\infty}} \right)}{\mu} \quad (5)$$

Thus, based on the semi-empirical equation developed by Prandtl-Schlichting, modified with the turbulent correction factor, the local skin friction drag coefficient can be calculated as:

$$C_{F_x} = \frac{0.455}{(\log_{10} Re_x)^{2.58}} - \frac{1700}{Re_x} \quad (6)$$

The total skin friction C_{D_0} can then be determined by summing all the skin friction coefficients of each cell. Therefore, the drag coefficient is calculated by the solver using:

$$C_D = C_{D_i} + C_{D_0} \quad (7)$$

The process of dividing the mesh implies an iterative process for evaluating the flow features. The solver ceased the process once the solution has converged to a criterion that can be defined by the user [11]. Unlike volume-based CFD solvers, FlightStream can produce flow solutions using an unstructured surface mesh, reducing significantly the time and the computational resources needed to generate solutions [12].

The latest version of the solver features a new physics-based viscous-coupled flow solver that enhanced the existing flow separation modelling used by FlightStream [13]. At high-lift incidence angles, increased coupling between the potential regions of the flow and the viscous boundary layer causes substantial flow non-linearity [14]. The driving force in this regime is therefore the displacement of the potential flow boundary by the high thickness of the viscous boundary layer. This effect leads to an overprediction of the aerodynamic forces by the current model [15].

Therefore, two models for the boundary layer computation have been implemented: laminar and turbulent. The laminar boundary layer computation method relies on the standard two-parameter model of the Thwaites integral method with the momentum integral equation, defined as :

$$U \frac{d}{d\eta} \left[\frac{\theta^2}{\nu} \right] = 0.45 - 6 \frac{\theta^2}{\nu} \frac{dU}{d\eta} \quad (8)$$

A new turbulent boundary layer model has been implemented, using the original model developed by Standen with several numerical improvements [16]. It is coupled with a modified numerical approach. The boundary layer is computed inside the potential flow solver. Then, the displacement of dividing streamlines, due to the flow non-linearity at high-lift incidence angles, is simulated by applying a blowing velocity V_N on the local slip-wall boundary, defined as:

$$V_N = \frac{\partial(U_e \delta^*)}{\partial s} \quad (9)$$

Here, δ^* is the displacement thickness, U_e the local streamline velocity outside the boundary layer and s the direction along the local surface.

The next iteration is then solved using updated boundary conditions with a modified slip-wall boundary. The iteration process is repeated until the convergence of the parameters.

The presence of both laminar and turbulent separation models allows the solver to model complex transitional separation physics along a given surface streamline [17].

Thus, FlightStream has been able so far to accurately predict the aerodynamic loads for an aircraft flying at subsonic speed. However, the use of this solver is limited to subsonic inviscid flow or attached boundary layer flow study. Therefore, for a delta wing where vortices play a major role in generating forces, the solver will need a complementary method to model the additional influence of the vortices over the aerodynamic loads.

VI. Complementary Method to Model Vortices

A. The Polhamus Method

One of the main issues associated with the prediction of the lift force of a delta wing is the estimation of the vortex lift, associated with the leading-edge vortex. The problem lies in the difficulty of accurately predicting the shape, the strength and the position of the vortex sheet [18].

The Polhamus method can avoid these issues by assuming a similarity between the additional normal force produced by the vortex flow and the leading-edge suction induced by a potential flow on a thin wing. Indeed, it is assumed that the forces needed to maintain the flow attached around a large leading-edge radius can be assimilated to the total force required to maintain the flow's equilibrium over a separated vortex sheet. Therefore, the normal force acting on the wing by the potential flow, which corresponds to the leading-edge suction, would be equivalent to the normal force associated with the vortex, from which the induced vortex lift can be determined. Figure 5 illustrates this assumption. Further details of the method are explained in Ref. [18].

It is assumed that the flow goes around the fully developed vortex and reattaches to the upper surface of the wing. Therefore, the overall generated lift force can be divided into two components:

- A lift force associated with a potential flow acting over a curved surface
- A vortex lift corresponding to the normal force needed to maintain the potential flow's equilibrium over a separated vortex sheet.

Since FlightStream can calculate accurately the forces induced by a potential flow over a lifting surface, the Polhamus method is used to estimate the additional component of lift over a delta wing, when a leading edge vortex appears [19].

According to the Polhamus method, the vortex lift coefficient can be defined as:

$$C_{L_V} = K_V \sin^2 \alpha \cos \alpha \quad (10)$$

Where K_V is the constant of proportionality in the vortex lift equation. The value of K_V can be determined using the graph created by Polhamus, expressing K_V as a function of the aspect ratio AR, as shown in Fig. 6.

Thus, the total lift coefficient can be calculated as:

$$C_{L_{total}} = C_{L_{FlightStream}} + C_{L_V} \quad (11)$$

Furthermore, the additional drag, caused by the vortex suction that comes with the fully developed vortex, can be defined as:

$$\Delta C_D = C_{L_{total}} \tan \alpha \quad (12)$$

When considering a potential flow, the additional drag ΔD is the amount of the induced drag produced by a thin wing. Therefore, the value of ΔC_D should replace the value of C_{D_i} estimated by the solver, in the calculation of the total drag.

Therefore, Eq. 7 should be modified to:

$$C_D = \Delta C_D + C_{D_0} \quad (13)$$

The strength of the Polhamus method is its simplicity to implement in any aerodynamic model, while it has consistently shown an excellent agreement with the experimental data for a delta wing.

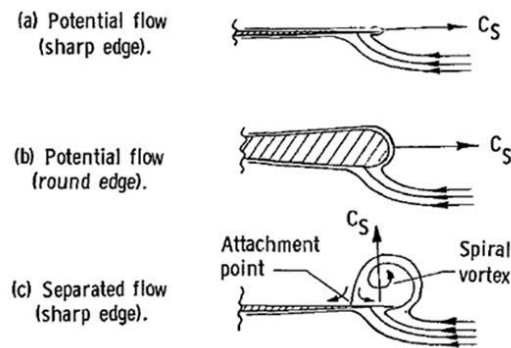


Fig. 5 Leading-edge flow conditions and the Polhamus Leading Edge Suction theory [10].

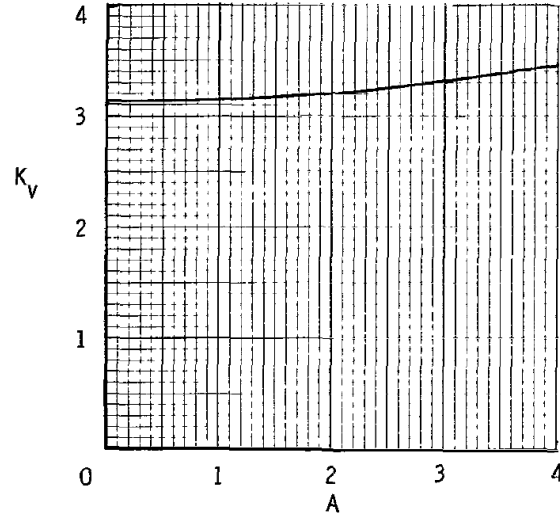


Fig. 6 Variation of K_v with AR for delta wings [18].

B. Flow Classification

To enhance the accuracy of the aerodynamic model, where FlightStream predictions are corrected using the Polhamus method, the use of such semi-empirical method should be limited to flow conditions where vortices are developed over the delta wing. Therefore, the application of the Polhamus theory is coupled with the flow classification, created by Miller and Wood [20]. The understanding and characterization of flows around delta wings have been experimentally studied with multiple leading-edge sweep angles and different techniques, within a large range of velocities up to hypersonic. Therefore, based on two parameters, the components of the angle of attack α_N and Mach Number M_N , both normal to the leading-edge, they were able to experimentally predict the flow pattern over a sharp-leading-edge delta wing [21]. These components are represented in Fig. 7 and can be mathematically defined as:

$$\alpha_N = \tan^{-1} \left(\frac{\tan \alpha}{\cos \Lambda_{LE}} \right) \quad (14)$$

$$M_N = M \cos \Lambda_{LE} \sqrt{1 + \sin^2 \alpha \tan^2 \Lambda_{LE}} \quad (15)$$

where Λ_{LE} is the leading-edge sweep angle, M the Mach Number and α the angle of attack.

Through flow visualizations and experimental observations, they were able to define seven categories of flow patterns identified as classical vortex (I), vortex with shock (II), separation bubble with shock (III), shock-induced separation (IV), shock without separation (V), separation bubble with no shock (VI) and no shock and no separation (VII). Figure 8 shows the flow patterns classification.

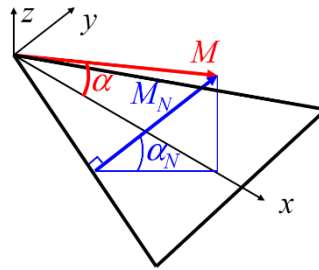


Fig. 7 Definition of α_N and M_N [21].

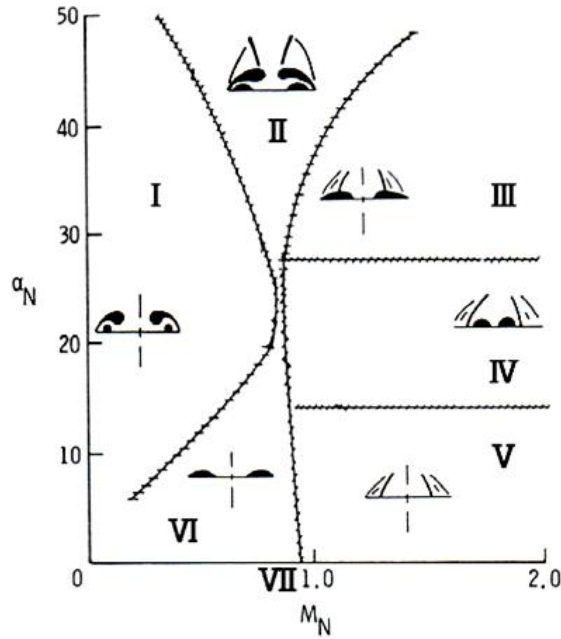


Fig. 8 Flow patterns classification chart [20].

Therefore, the correction method consists in first determining the flow pattern over the wing for the current flow conditions (Mach number and angle of attack), using the Miller & Wood flow classification. If it falls within the range of the pattern “separation bubble with no shock (VI)”, a classic lifting-surface theory can be applied to estimate aerodynamic forces accurately, without the need to correct the results. For this flow pattern, FlightStream can deliver accurate results. If it falls within the range of the pattern “classical vortex (I)”, the Polhamus method can be applied, since a vortex sheet will be present. The additional lift and drag components can be added to the initial FlightStream’s predictions.

VII. Preliminary Results

The first case is based on the ONERA wind tunnel test campaign which provided experimental results performed in a low subsonic wind tunnel, at a Mach Number of $M = 0.133$ and at a Reynolds Number of $Re_{mac} = 10^6$, for a range of angles of attack of $[-8^\circ; 40^\circ]$ [5]. Aerodynamic forces were expressed as axial and normal force coefficients. Therefore, the drag and lift coefficients can be calculated using the following transformations:

$$C_L = C_N \cos \alpha - C_A \sin \alpha \quad (16)$$

$$C_D = C_N \sin \alpha + C_A \cos \alpha \quad (17)$$

Under the same flow conditions, numerical data were computed with FlightStream and compared against experimental data, as shown in Fig 9 and 10. Using the Miller & Wood flow classification, it has been determined that, under current flow conditions, the first appearance of the primary vortex at the apex would theoretically be at 2° of AoA. It can be observed that before this angle, initial FlightStream results match very well with the experimental data, confirming the accuracy of the solver. However, above 2° of AoA, it can be noticed that FlightStream results gradually diverged from the reference data, as the solver is not able to model the growing vortex influence over the aerodynamic forces. At 22° of AoA, the solver is predicting the wing stall, which does not conform with the experimental observations due to the presence of vortices, delaying its stall to 36° of AoA. Flow solutions were computed and the pressure contours, in Fig. 12, were compared against RANS solver results in Fig. 11, for a flow at three different angles of attack and at a Mach Number of $M = 0.2$. The streamlines, modelled by the FlightStream solver, are represented in Fig. 13. This demonstrates the absence of any vortex captured by the FlightStream solver, since there is no suction trace in pressure distribution and the streamlines do not show any swirling motion of the flow.

Therefore, the Polhamus method is applied as a correction from 2° of AoA. While it has been experimentally observed that the primary vortex appeared at 6° of angle of attack, the difference can be explained by the fact that the flow classification has been created based on the collection of experimental data and observation, and therefore is not exact. Between 2 and 6° , the vortices are still weak, and thus their influence over the aerodynamic forces is still negligible.

Excellent agreement is obtained between the corrected data and the experimental results for all angles of attack up to 36° , where the stall of the wing is observed due to the vortex burst. The Polhamus method is unable to predict this phenomenon, which is one of the limitations of such a method.

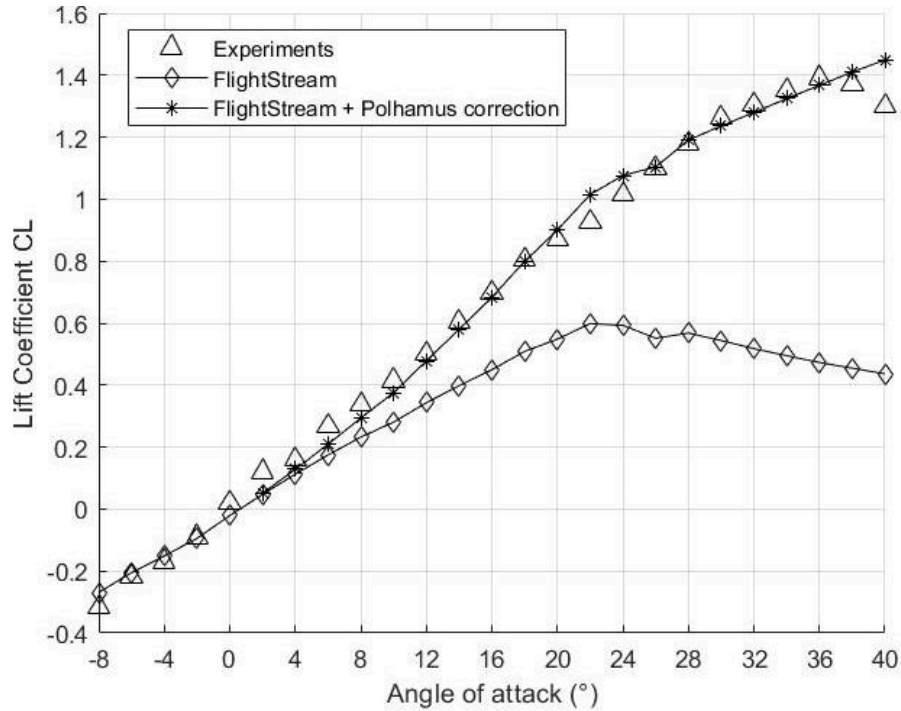


Fig. 9 Lift Polar for a subsonic flow at $M = 0.133$ and at $Re_{mac} = 10^6$.

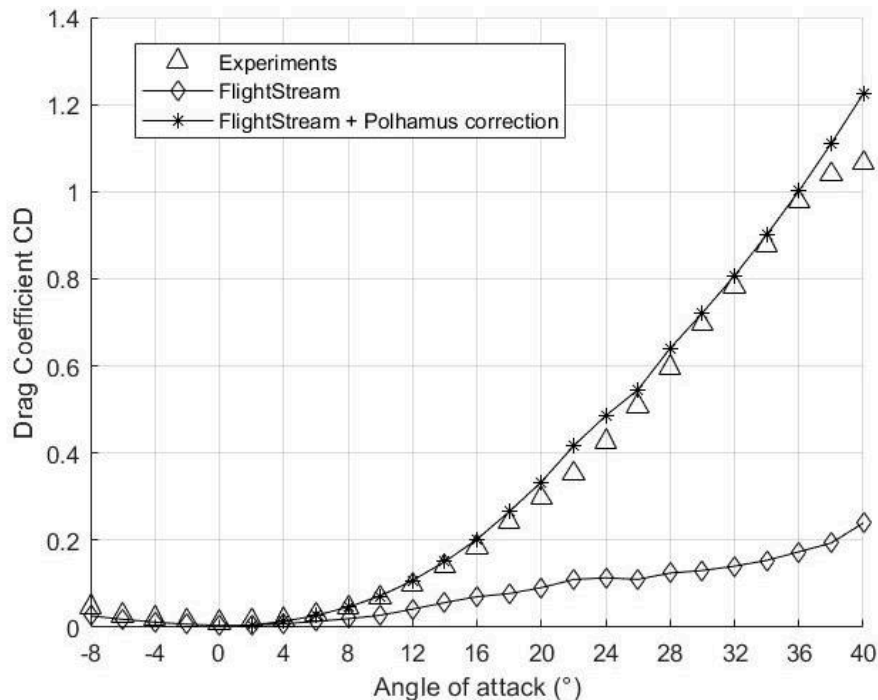


Fig. 10 Drag Polar for a subsonic flow at $M = 0.133$ and at $Re_{mac} = 10^6$.

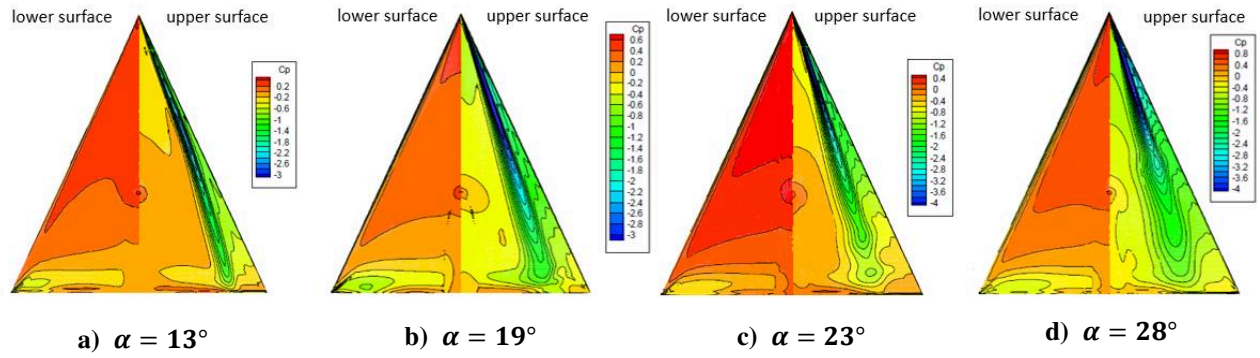


Fig. 11 Pressure contour for a flow at $M = 0.2$ and at $Re_{mac} = 2.13 \times 10^6$, using RANS solver [4].

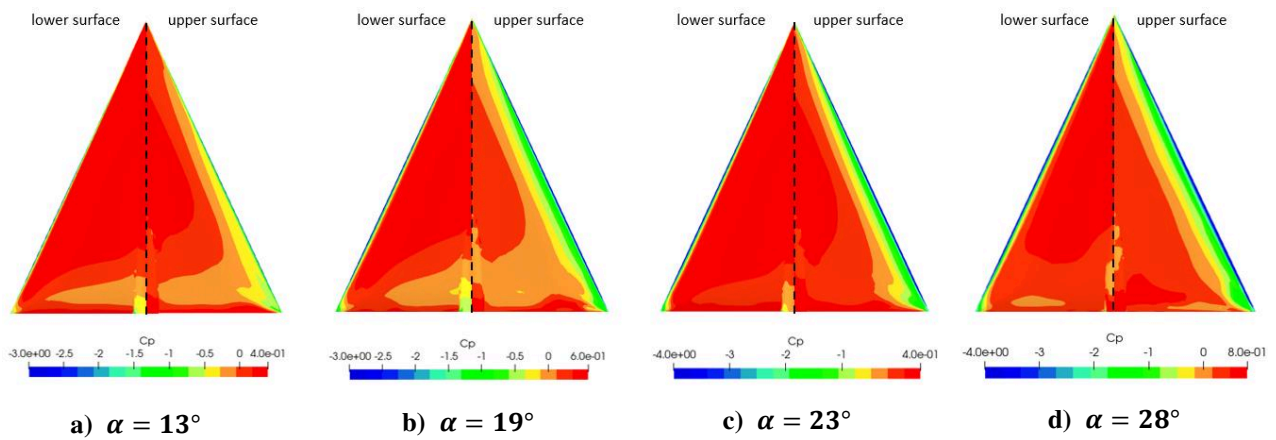


Fig. 12 Pressure contour for a flow at $M = 0.2$ and at $Re_{mac} = 2.13 \times 10^6$, using FlightStream solver.

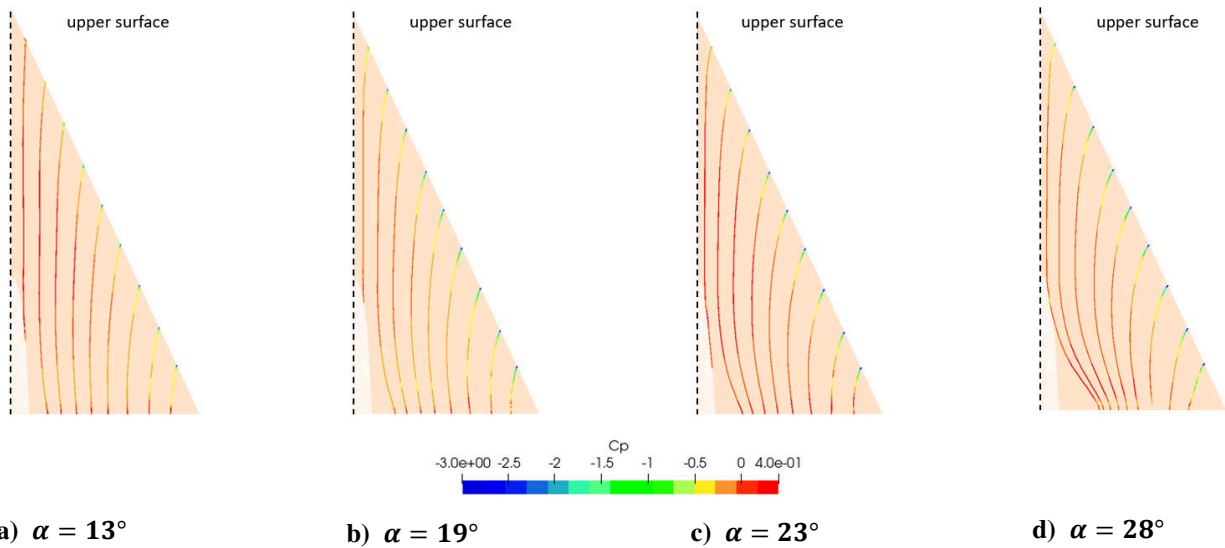


Fig. 13 Streamlines in function of pressure distribution for a flow at $M = 0.2$ and at $Re_{mac} = 2.13 \times 10^6$, using FlightStream solver.

VIII. Aspect Ratio and Sweep Angle Sensitivity Analysis

The R.A.E [Ref] test campaign provided experimental results performed in a low turbulence wind tunnel, for a family of six cambered delta wings having sharp leading edges, with various aspect ratios and sweep angles as detailed in Fig. 3 and Table. 2. The test campaign was performed at a fixed velocity of $V = 100 \text{ ft/sec}$ for a range of different Reynolds numbers, based on the aerodynamic mean chord, from $Re_{mac} = 0.25 \times 10^6$ to $Re_{mac} = 0.5 \times 10^6$. The range of angle of attack considered for measurements was $[-60^\circ; 60^\circ]$. The variation of lift with incidence and the variation of drag with lift were provided. Under the same flow conditions, a similar methodology was used as dewscribed in Part VII, to compute numerical data with FlightStream and to compare it with experimental data.

It can be observed that for the 45° swept delta wing, the FlightStream solver appears to be accurate enough, without any need for further correction, as the computed data match well the experimental data, up to the wing stall. It appears that for a low sweep angle, the amount of lift force produced by the vortices is minor. This is consistent with the experimental analysis and the expected flow pattern. It has been observed experimentally that for the 45° swept delta wing, the vortex breakdown point was close to the wing’s apex [7]. The detached vortex has consequently less intensity. Due to the weaker vortex, a significant reduction in vortex lift is induced in regions where the primary vortex has detached from the leading edge. With only a small amount of vortex lift produced, the FlightStream solver is sufficient to capture the aerodynamic forces.

For the remaining wings, it has been experimentally established that the position of the vortex breakdown point moves forward as the incidence increases and the sweep angle decreases [7]. Since the Polhamus method is not able to capture the effect of the vortex breakdown on the aerodynamic forces, its position plays a major role in the accuracy of the overall correction method. For the 55° and 60° swept delta wings, it has been observed that the vortex breakdown occurred at respectively $0.85c$ for 13° of AoA and $0.7c$ for 15° of AoA. Thus, for these two delta wings, a good match is observed between experimental and computed data up to 15° of AoA. Above this incidence, the vortex breakdown happens and leads to a reduction in lift. Therefore, The Polhamus method which is unable to model the effect of the vortex breakdown, is overestimating the lift force, leading to increasing differences with the experimental data.

As for the 65° , 70° and 76° swept delta wings, the vortex breakdown occurs at a point closer to or after the trailing-edge. Consequently, this phenomenon leads to minor disruption in the flow pattern over the delta wing. As a result, an excellent agreement is observed between experimental data and simulated data from FlightStream Solver coupled with the Polhamus method, up until the wing stall due to the vortex burst.

In conclusion, the accuracy of the correction method is sensitive to the sweep angle and the aspect ratio of the wing. These two parameters will directly affect the position of the vortex breakdown which leads to a reduction in lift. As the Polhamus method is unable to capture its effect, the correction method accuracy relies on clean flow patterns that are not disturbed by the vortex breakdown, i.e. for wings with high sweep angles and low aspect ratios.

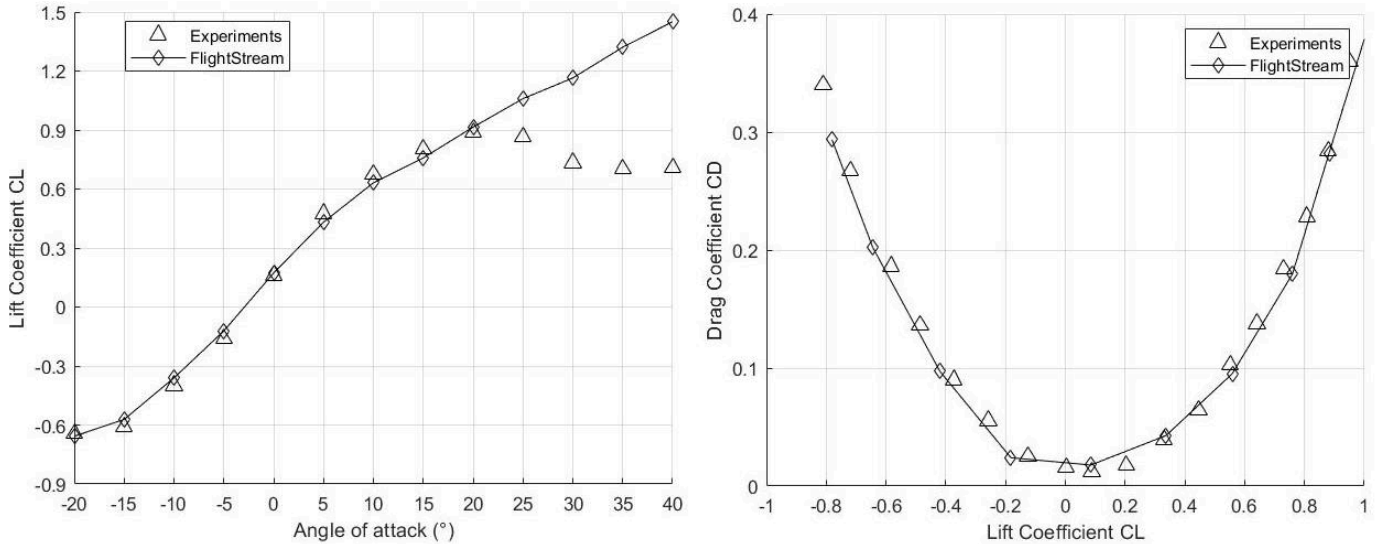


Fig. 14 Lift and Drag Polar for a subsonic flow at $V = 100 \text{ ft/sec}$ and at $Re_{mac} = 0.25 \times 10^6$ for a 45° swept delta wing.

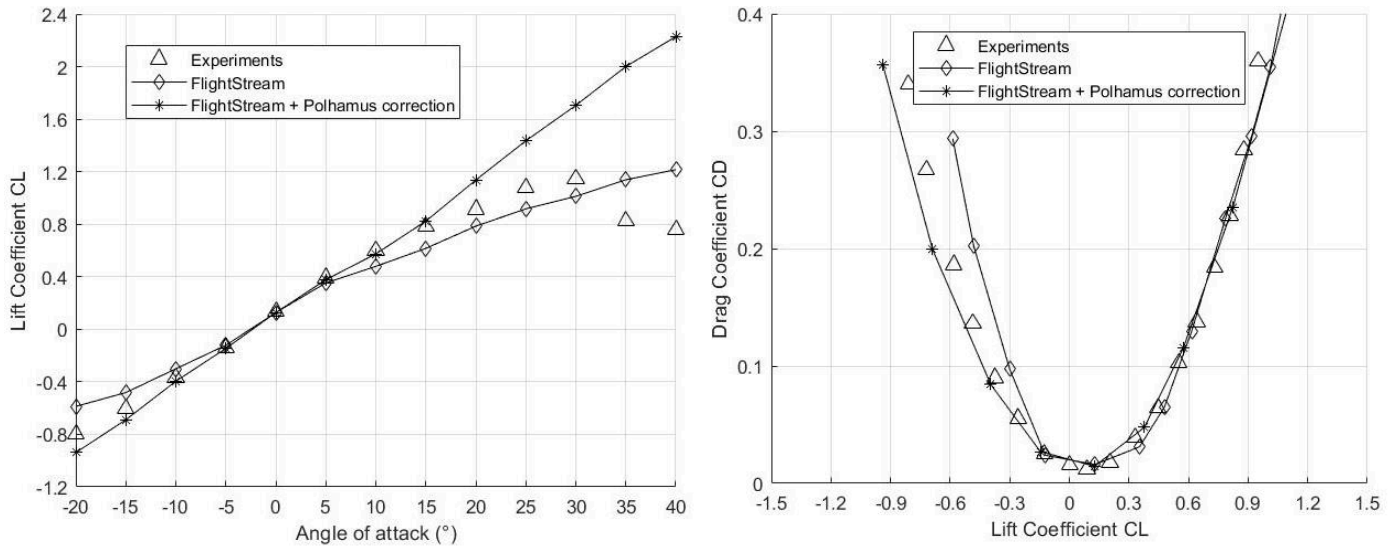


Fig. 15 Lift and Drag Polar for a subsonic flow at $V = 100 \text{ ft/sec}$ and at $Re_{mac} = 0.3 \times 10^6$ for a 55° swept delta wing.

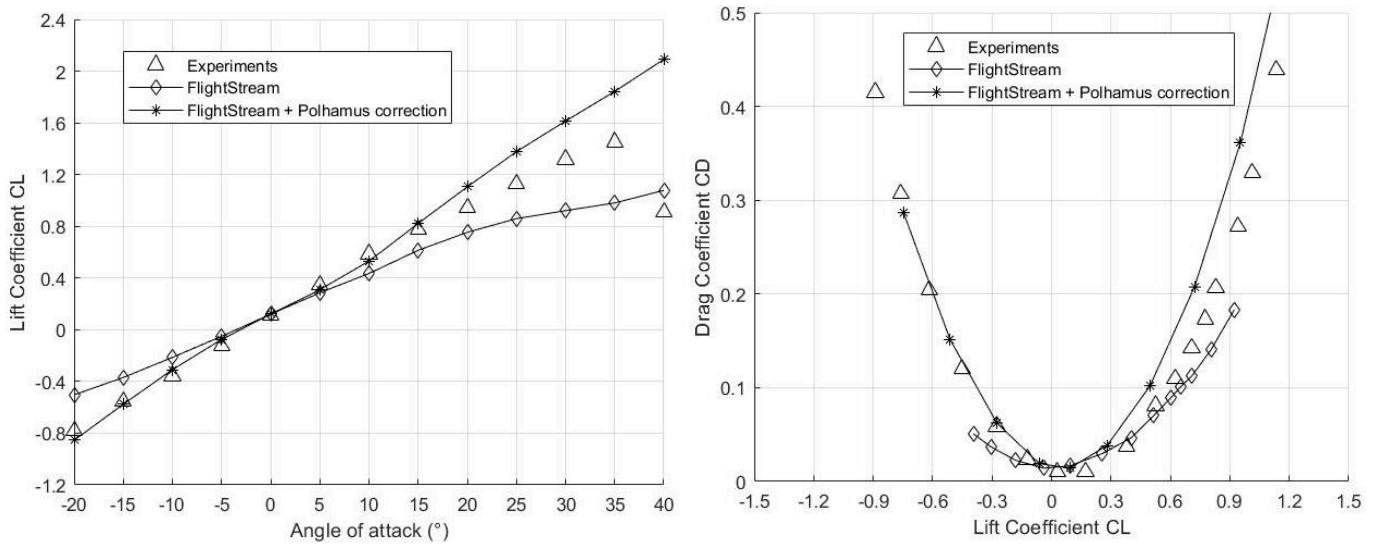


Fig. 16 Lift and Drag Polar for a subsonic flow at $V = 100 \text{ ft/sec}$ and at $Re_{mac} = 0.33 \times 10^6$ for a 60° swept delta wing.

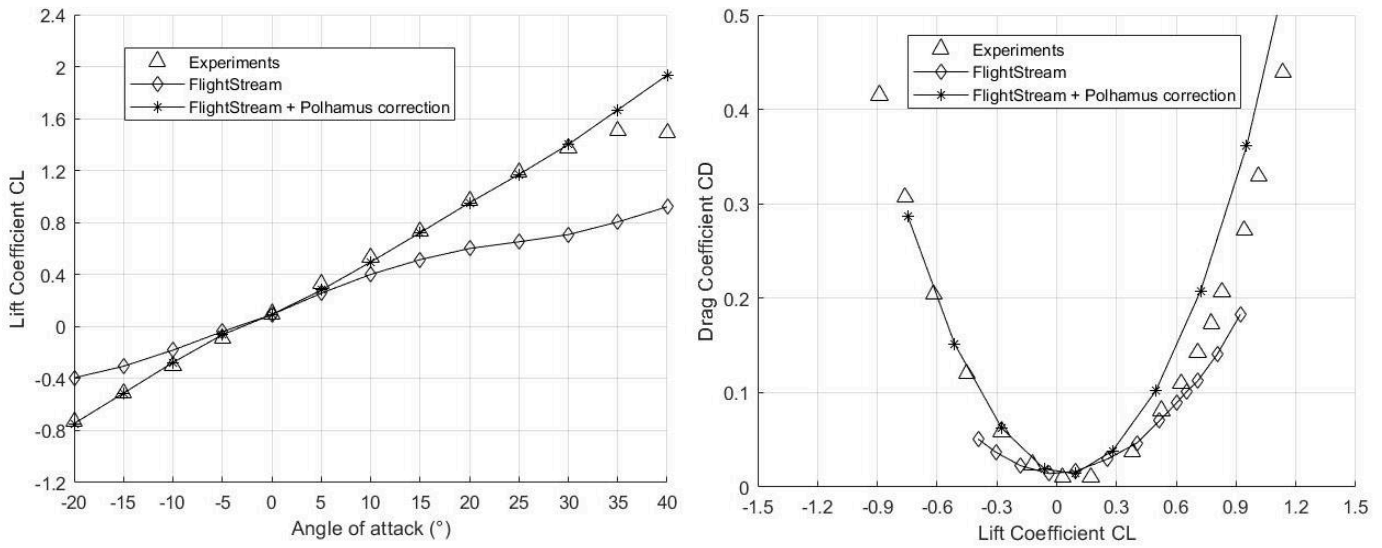


Fig. 17 Lift and Drag Polar for a subsonic flow at $V = 100 \text{ ft/sec}$ and at $Re_{mac} = 0.37 \times 10^6$ for a 65° swept delta wing.

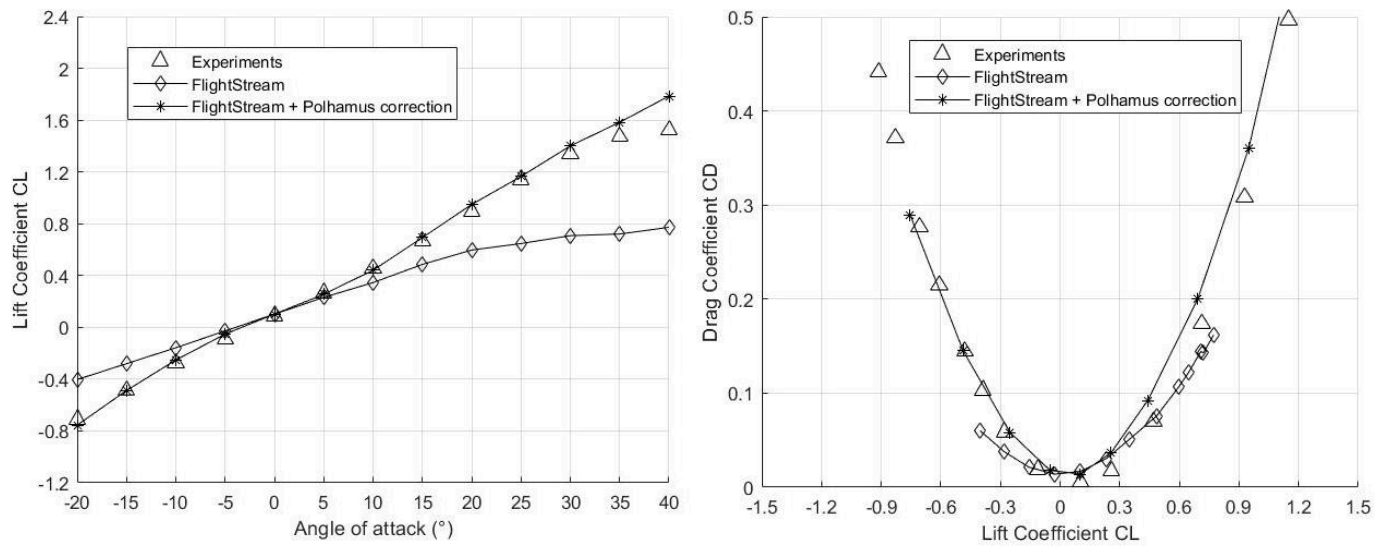


Fig. 18 Lift and Drag Polar for a subsonic flow at $V = 100 \text{ ft/sec}$ and at $Re_{mac} = 0.42 \times 10^6$ for a 70° swept delta wing.

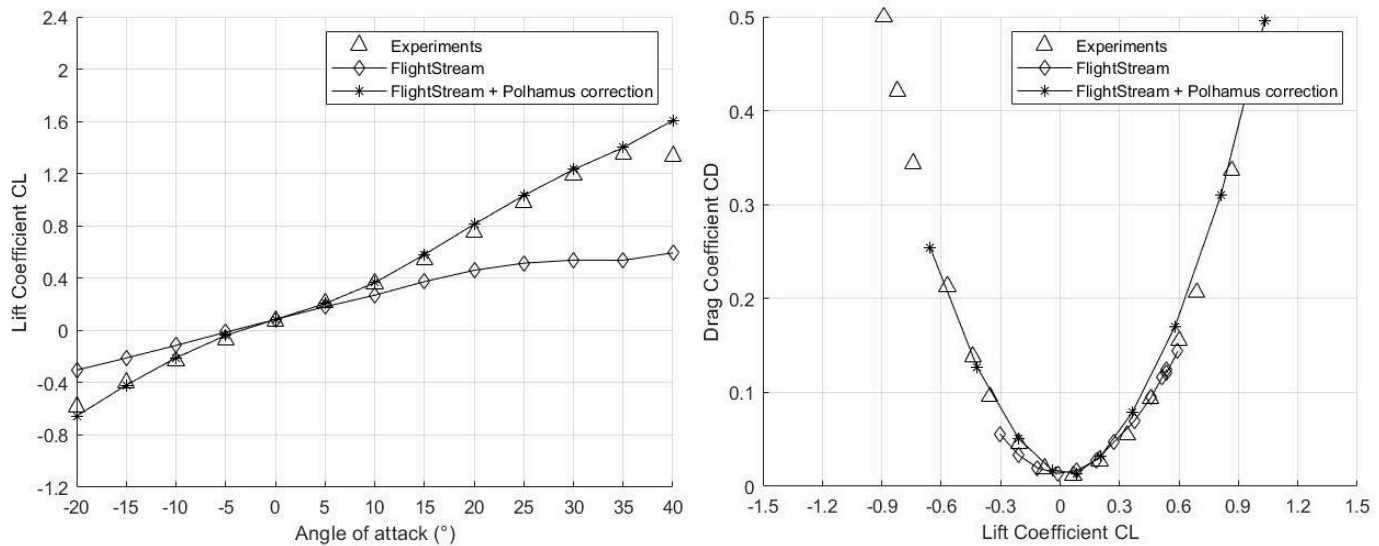


Fig. 19 Lift and Drag Polar for a subsonic flow at $V = 100 \text{ ft/sec}$ and at $Re_{mac} = 0.5 \times 10^6$ for a 76° swept delta wing.

IX. Computational Resources

The strength of the FlightStream solver is its notable efficiency and rapidness for computing potential flows. Indeed, for a range of $[-20^\circ; 40^\circ]$ of AoA, it only required less than 300 sec to generate the global aerodynamic data for 13 different calculations using a desktop computer with 3 CPUs. The solver needs less than 10 000 cells for the geometry's mesh to accurately capture the flow features. Therefore, these properties make the solver particularly suitable and adapted for conceptual and preliminary aerodynamic design studies, with a strong need for a high number of iterations. With low computational resources, FlightStream can accurately model the aerodynamic forces of a potential flow. Coupled with the Polhamus method, its domain can be extended to vortex flows.

X. Conclusion

FlightStream solver coupled with the correction method, based on the application of the Polhamus method, has been shown to be accurate in modelling aerodynamic forces over a 65° delta wing for the full range of angle of attack until the wing stall. The solver coupled with the Polhamus method has demonstrated to be particularly accurate for low aspect ratio and highly swept delta wings. Nevertheless, the correction method shows its limitations when the vortex breakdown occurs, resulting in a loss in lift.

The sensitivity analysis against sweep angle has demonstrated that the position of the vortex breakdown point along the wing plays a major role in the accuracy of such method. Indeed, as the sweep angle increases, the position of the vortex breakdown moves backward. Therefore, for flow conditions where the vortex breakdown happens right over the wing, thus disrupting the flow pattern, the Polhamus Method is unable to predict the change in aerodynamic forces, losing in accuracy.

The FlightStream modelling properties, easy to apply and fast to compute flow solutions within a few minutes, make it well adapted for preliminary and conceptual design of delta wings, without requiring high computational resources nor large amounts of time. The FlightStream solver, coupled with the Polhamus Method for specific conditions identified thanks to the Miller & Wood Classification, has demonstrated to be accurate in predicting aerodynamic forces generated by a subsonic vortex flow, up to the vortex burst.

Acknowledgements

The author wishes to acknowledge the cooperation and support of Dr Davide di Pasquale, Dr Simon A. Prince and Dr Vivek Ahuja along the work. Their guidance and assistance were particularly precious during the process. The author wishes to also thank Johan Gabriel Vargas and Matthieu Deyries for their unconditional support and assistance.

References

- [1] J. M. Luckring, "The discovery and prediction of vortex flow aerodynamics," *Aeronautical Journal*, vol. 123, no. 1264, pp. 729–804, Jun. 2019.
- [2] M. Gad-El-Hak, *Frontiers in Experimental Fluid Mechanics*. Springer Science and Business Media LLC, 1989.
- [3] I. Heron and R. Y. Myose, "Delta wing vortex-burst behavior under a dynamic freestream," *Journal of Aircraft*, vol. 46, no. 5, pp. 1500–1512, 2009.
- [4] J. M. Luckring, "Reynolds Number, Compressibility, and Leading-Edge Bluntness Effects on Delta-Wing Aerodynamics," *24th International Congress of the Aeronautical Sciences*, Oct. 2004.
- [5] J. F. le Roy, O. Rodriguez, and S. Kurun, "Experimental and CFD contribution to delta wing vortical flow understanding," *46th AIAA Aerospace Sciences Meeting and Exhibit*, no. January, pp. 1–12, 2008.
- [6] J. M. Luckring, "Initial experiments and analysis of blunt-edge vortex flows for VFE-2 configurations at NASA Langley, USA," *Aerospace Science and Technology*, vol. 24, no. 1, pp. 10–21, 2013
- [7] P. B. Earnshaw and J. a Lawford, "Low-Speed Wind-Tunnel Experiments on a Series of Sharp-Edged Delta Wings," *Aeronautical Research Council-Reports and Memoranda*, no. 3424, 1964.
- [8] J. Quitter, M. Marino and J. Bauschat, "Highly Non-Planar Aircraft Configurations: Estimation of Flight Mechanical Derivatives Using Low-Order Methods," *Deutscher Luft- und Raumfahrtkongress, DLRK 2019*.
- [9] V. Ahuja, R. J. Hartfield and D. Ciliberti, "Three-dimensional Viscous Coupling & Flow Separation Enhancements to an Inviscid Surface Vorticity Flow Solver," 2022.
- [10] V. Ahuja and R. J. Hartfield, "Aerodynamic loads over arbitrary bodies by method of integrated circulation," *Journal of Aircraft*, vol. 53, no. 6, pp. 1719–1730, 2016.
- [11] V. Ahuja, J. Burkhalter and R. J. Hartfield, "Robust prediction of high lift using surface vorticity," Austin: NASA SBIR NNX17CL12C, Phase II final report, 2017.
- [12] M. F. M. Hoogreef and J. S. E. Soikkeli, "Flight dynamics and control assessment for differential thrust aircraft in engine inoperative conditions including aero-propulsive effects," *CEAS Aeronautical Journal*, 2022.
- [13] F. A. Dvorak, B. Maskew and F. A. Woodward, "Investigation of Three-Dimensional Flow Separation on Fuselage Configurations", Analytical Methods, Inc., USAAMRDLTR-77-4, March 1977.
- [14] K. A. Deere, S. A. Viken, M. B. Carter, J. K. Viken and J. M. Derlaga, "Comparison of High-Fidelity Computational Tools for Wing Design of a Distributed Electric Propulsion Aircraft", 35TH AIAA Applied Aerodynamics Conference, 5-9 June 2017.
- [15] G. A. DiMaggio, R. J. Hartfield and V. Ahuja, "Rapid Prediction of Hybrid Wing Body Aerodynamics" AIAA AVIATION Forum, 2022.
- [16] A. S. Olsen, N. R. Garcia and C. Bak, "Improved Roughness Model for Turbulent Flow in 2D Viscid-Inviscid Panel Methods," *Journal of Wind Energy*, October 2019
- [17] C. L. Merkle, T. Kubota and D. R. S. Ko, "An Analytical Study of the effects of Surface Roughness on Boundary-Layer Transition", Air Force Office of Scientific Research, AD/A-004 786, October, 1974.
- [18] E. C. Polhamus, "A concept of the vortex lift of sharp-edge delta wings based on a leading-edge-suction analogy," *NASA Technical Note D-3767*, 1966.
- [19] E. C. Polhamus, "Application of the leading-edge-suction analogy of vortex lift to the drag due to lift of sharp-edge delta wings," *NASA technical note D-4739*, 1968.
- [20] D. S. Miller and R. M. Wood, "Leeside flows over delta wings at supersonic speeds," *Journal of Aircraft*, vol. 21, no. 9, pp. 680–686, 1984.
- [21] A. Oyama, G. Imai, A. Ogawa, and K. Fujii, "Aerodynamic characteristics of a delta wing at high angles of attack," *15th AIAA International Space Planes and Hypersonic Systems and Technologies*, 2008. doi: 10.2514/6.2008-2563.